Author/s:
Guo, J;Wang, X;Henstridge, DC;Richardson, JJ;Cui, J;Sharma, A;Febbraio, MA;Peter, K;de Haan, JB;Hagemeyer, CE;Caruso, F

Title:
Nanoporous Metal–Phenolic Particles as Ultrasound Imaging Probes for Hydrogen Peroxide

Date:
2015-10-01

Citation:
Guo, J., Wang, X., Henstridge, D. C., Richardson, J. J., Cui, J., Sharma, A., Febbraio, M. A., Peter, K., de Haan, J. B., Hagemeyer, C. E. & Caruso, F. (2015). Nanoporous Metal–Phenolic Particles as Ultrasound Imaging Probes for Hydrogen Peroxide. Advanced healthcare materials, 4 (14), pp.2170-2175. https://doi.org/10.1002/adhm.201500528.

Persistent Link:
https://hdl.handle.net/11343/90853

DOI: 10.1002/((please add manuscript number))
Article type: Communication

Nanoporous Metal-Phenolic Particles as Ultrasound Imaging Probes for Hydrogen Peroxide

Junling Guo, Xiaowei Wang, Darren C. Henstridge, Joseph J. Richardson,[†] Jiwei Cui, Arpeeta Sharma, Mark A. Febbraio, Karlheinz Peter, Judy B. de Haan, Christoph E. Hagemeyer,[*] and Frank Caruso[*]

J. Guo, Dr. J. J. Richardson, Dr. J. Cui, Prof. F. Caruso
ARC Centre of Excellence in Convergent Bio-Nano Science and Technology, and the Department of Chemical and Biomolecular Engineering, The University of Melbourne, Parkville, Victoria 3010, Australia. E-mail: fcaruso@unimelb.edu.au

Dr. X. Wang, Prof. K. Peter
Atherothrombosis and Vascular Biology, Baker IDI Heart and Diabetes Institute, Melbourne, Victoria 3004, Australia.

Dr. X. Wang, Prof. K. Peter, Prof. C. E. Hagemeyer
Central Clinical School, Monash University, Melbourne, Victoria 3004, Australia.

A. Sharma, A/Prof. J. B. de Haan
Oxidative Stress, Baker IDI Heart and Diabetes Institute, Melbourne, Victoria 3004, Australia.

Dr. D. C. Henstridge, Prof. M. A. Febbraio
Cellular and Molecular Metabolism, Baker IDI Heart and Diabetes Institute, Melbourne, Victoria 3004, Australia.

Prof. K. Peter, Prof. C. E. Hagemeyer
School of Applied Sciences, RMIT University, Melbourne, Victoria 3000, Australia.

Prof. C. E. Hagemeyer
Vascular Biotechnology, Baker IDI Heart and Diabetes Institute, Melbourne, Victoria 3004, Australia. E-mail: christoph.hagemeyer@bakeridi.edu.au

† Present address: CSIRO Manufacturing Flagship, CSIRO, Clayton South, Victoria 3169, Australia

Keywords: hydrogen peroxide, metal-phenolic particles, ultrasound imaging

Hydrogen peroxide (H_2O_2) is a reactive oxygen species (ROS) produced endogenously that is required for various physiological processes (e.g., host defense). H_2O_2 is also an important second messenger in signal transduction pathways.[1] These beneficial aspects of H_2O_2 are counter-balanced by its hormetic effect, where H_2O_2 at higher concentrations is linked to various pathologies, such as diabetes, cardiovascular disease, renal injury, retinopathy, and cancer.[2] The overproduction of H_2O_2 can damage DNA, RNA, cellular lipids, and proteins, thereby inhibiting their normal physiological roles.

The detection of specific ROS, especially H_2O_2, has been achieved by using fluorescent molecular probes,[3] near-infrared imaging,[4] and electrochemical sensors.[5] However, limitations of these conventional methods, such as poor specificity, toxicity, complicated fabrication, non-biodegradable materials, as well as use of not readily available imaging modalities, and high-cost in clinical applications,[6] have hampered further clinical translational applications. This has resulted in a lack of easy and efficient methods to detect specific ROS *in vivo.* The lowering of pathological levels of H_2O_2 is also seen as a desirable therapeutic goal that may offer a means for lessening the pathological burden.[7] However, large scale clinical trials (HOPE, GISSI and Physicians Health Study II) failed, where the non-specific vitamins C and E demonstrated no additional benefits, and were actually linked to a worsening of cardiovascular disease outcomes.[8] Therefore, the development of improved methods for H_2O_2 detection is highly desirable, not only for the visualization of H_2O_2 production, but also for the development and testing of novel therapeutics capable of reducing H_2O_2 under pathological conditions.[2,7]

Among the different imaging modalities available in current clinical settings, ultrasound imaging technology (US) offers significant advantages, such as easy access, non-ionizing radiation,[9] low-cost, portability,[10] and real-time imaging, thereby making it well suited to routine clinical applications,[11] such as screening and early disease detection.[12] US imaging has been improved with the use of contrast agents, such as microbubbles (MBs), and research into molecular US imaging is ongoing.[13] Recently, we showed that a common natural phenolic,

tannic acid (TA, **Figure S1**), can be used to coordinate different metals, across the periodic table, through a rapid assembly process, thereby establishing a broad library of metal-phenolic network (MPN) films and capsules. The functional properties of MPN materials, such as biodegradation, fluorescence, and multimodal imaging, can be easily tailored through the choice of the metals used for complexation.[14] These MPNs represent a platform for engineering advanced US contrast agents, including the detection of H_2O_2 in biological and/or biomedical applications.

Herein, we report the development of nanoporous metal-phenolic particles that are capable of probing endogenous levels of H_2O_2 by US imaging *in vitro*, *ex vivo* and *in vivo*. These particles (nanoporous Fe^{III}-TA replica particles, denoted *np*Fe^{III}-TA RPs) are engineered by the nanostructural replication of nanoporous calcium carbonate (*np*$CaCO_3$) particles filled with Fe^{III}-TA complexes (**Figure 1a**). The Fe^{3+} chelated by the phenolic ligand possesses catalytic activity that converts H_2O_2 into oxygen (O_2) molecules under physiological pH (**Figure 1b**). Under pathological conditions, tissues produce elevated levels of H_2O_2, and this H_2O_2 can be activated by the *np*Fe^{III}-TA RPs to generate MBs of O_2, thereby changing the acoustic impedance and creating specific non-linear oscillations, which can be detected by US imaging in real time (**Figure 1c**).[15] Wild-type (WT) and glutathione peroxidase-1 knockout ($GPx1^{-/-}$) mice were chosen as models to examine the potential of these *np*Fe^{III}-TA RPs in the detection of endogenous H_2O_2 *ex vivo* and *in vivo*. Compared with the previously reported lipopolysaccharide (LPS)-treated inflammatory model,[3,4] $GPx1^{-/-}$ mice are more clinically relevant, as they have been shown to be more susceptible to oxidant-mediated damage associated with endothelial dysfunction,[16] cardiovascular diseases (eg., atherosclerosis),[17] diabetic complications,[18] stroke,[19] traumatic brain injury,[20] and retinal diseases.[21] This study provides one of the few examples of the facile yet efficient formation of highly biocompatible nanostructured particles that are capable of rapidly detecting elevated levels of H_2O_2, and also demonstrates the potential use of metal-phenolic particles for advanced ultrasound imaging in biomedical research.

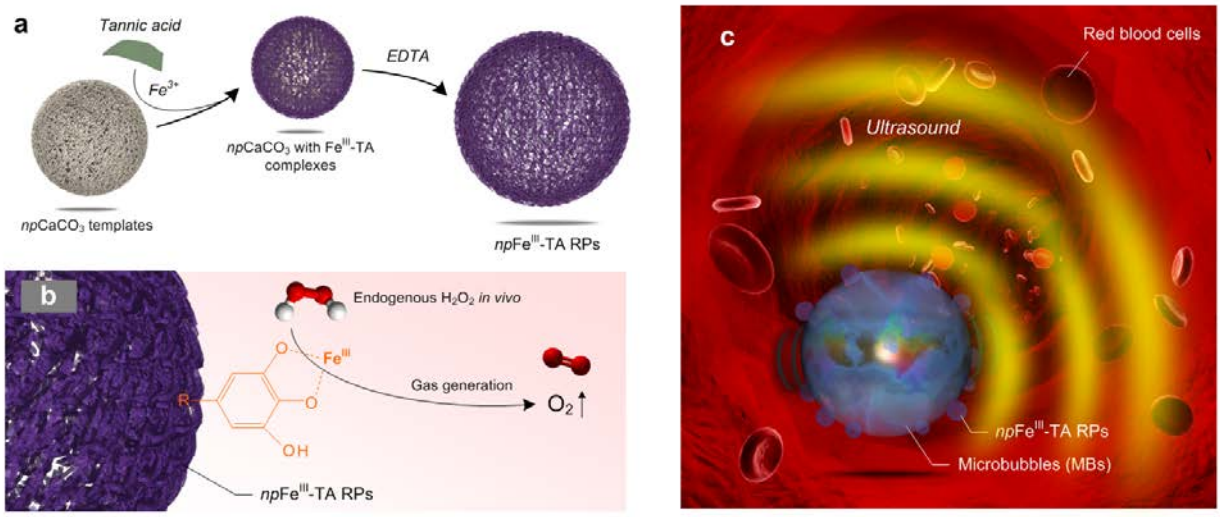

Figure 1. Schematic representation for the formation of *np*Fe^{III}-TA RPs for the formation of chemically generated microbubbles (MBs) to probe H_2O_2 *ex vivo* and *in vivo* by ultrasound (US) imaging. (a) The formation of *np*Fe^{III}-TA RPs by replication of *np*$CaCO_3$ template particles filled with Fe^{III}-TA complexes. (b) The interfacial reaction of H_2O_2, splitting to H_2O and O_2 with the catalytic assistance of chelated Fe^{3+} in the *np*Fe^{III}-TA RPs. (c) Gas nucleation of O_2 forms MBs, leading to changes of acoustic impedance in tissue; these changes can be detected by scanning the region of interest using US imaging.

The *np*Fe^{III}-TA RPs were formed by complexing TA and Fe^{3+} in *np*$CaCO_3$ particles, followed by removal of the templates (**Figure 2a**). The *np*$CaCO_3$ particles (**Figure S2**) were synthesized by calcination of poly(sodium styrene sulfonate) (PSS)-stabilized $CaCO_3$ particles, according to modified literature methods.[22] To facilitate the efficient filling of Fe^{III}-TA complexes into the *np*$CaCO_3$, TA solution was used to infiltrate the template particles, and then $FeCl_3$ solution and 3-(N-morpholino)propansulfonic acid (MOPS) buffer solution (pH 8.0) were sequentially added. Finally, the *np*$CaCO_3$ templates were removed by washing with ethylenediaminetetraacetic acid (EDTA) solution. The UV-Vis spectrum of the obtained *np*Fe^{III}-TA RPs showed a characteristic band at around 520 nm, which can be attributed to the charge transfer from the galloyl group of TA to chelated Fe^{3+} (**Figure S3**).[23] *np*Fe^{III}-TA RPs showed a spherical structure (**Figure 2b**), without collapse, after air drying, confirming that they are particles, and dissimilar to our previously reported Fe^{III}-TA capsules.[14] This difference can be the result of different nanostructures in the capsules and replica particles: Fe^{III}-TA capsules were formed from thin films of thickness ~10 nm,[14] while the *np*Fe^{III}-TA RPs were constructed with dense Fe^{III}-TA complex clusters (**Figure S4**). As shown in **Figure 2c-e**, the pore size of *np*Fe^{III}-TA RPs was measured to be 50.1 ± 18.8 nm (**Figure S5**), and this nanoporous structure can

facilitate the highly efficient interfacial reaction between the particles and H_2O_2, which results in a quick and highly sensitive reaction to breakdown H_2O_2 to O_2. High-angle annular dark-field (HAADF) images further confirmed the hollow and highly porous structures of the *np*Fe^{III}-TA RPs (**Figure 2f**). The corresponding energy dispersive X-ray (EDX) mapping analysis showed that the Fe distribution patterns matched well with the HAADF image and the distribution patterns of C and O maps. This confirmed that the Fe^{3+} were associated with TA and highly distributed in the particles acting as a series of highly efficient catalytic sites. The cytotoxicity of Fe^{III}-TA materials was found to be negligible.[14] Because of the highly porous structure, *np*Fe^{III}-TA RPs were also shown to have potential for the loading and delivery of therapeutic drugs (**Figure S6**).

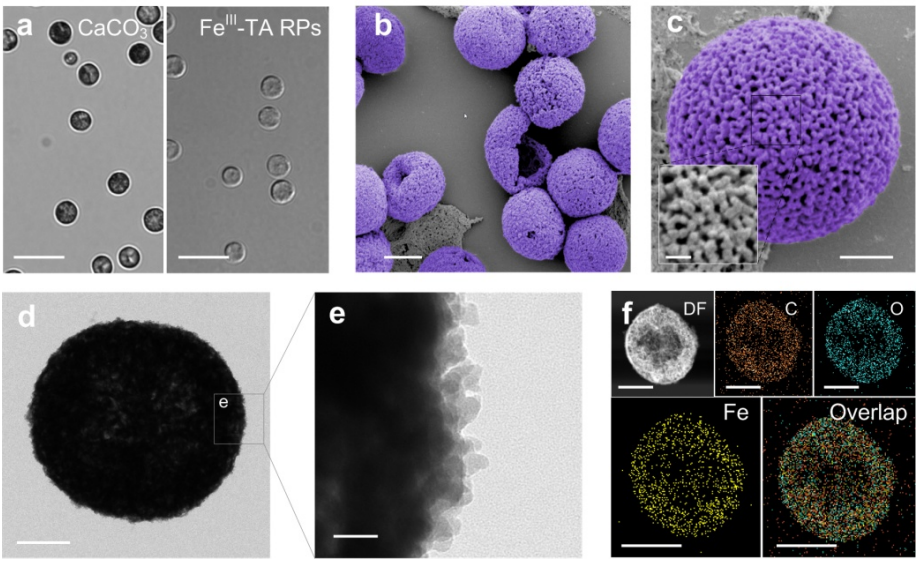

Figure 2. Structural characterization of *np*Fe^{III}-TA RPs. (a) Differential interference contrast (DIC) images of *np*$CaCO_3$ template particles and *np*Fe^{III}-TA RPs. (b) and (c) Scanning electron microscope images of *np*Fe^{III}-TA RPs with hollow structures. Inset of (c) shows the nanoporous networks. (d) and (e) Transmission electron microscopy images of *np*Fe^{III}-TA RPs with dense nanoclusters of Fe^{III}-TA complexes. (f) HAADF microscope image and corresponding EDX mappings of *np*Fe^{III}-TA RPs: dark field is represented as DF, carbon (C), oxygen (O), and iron (Fe). The scale bars are (a) 5.0 μm, (b) 1.0 μm, (c) 500 nm and 100 nm (inset), (d) 500 nm, (e) 100 nm, and (f) 1.0 μm.

To examine the ability of *np*Fe^{III}-TA RPs to generate O_2 MBs in the presence of H_2O_2, a H_2O_2 solution (pH 7.4, PBS buffer) was added into a suspension of *np*Fe^{III}-TA RPs (**Figure 3a**). Using the naked eye, it could be observed that small bubbles formed and merged into

bigger bubbles after 10 min. The generation process of the MBs was observed using differential interference contrast (DIC) microscopy. Initially, the MBs were ~5 μm in diameter, however as more O_2 was generated, the small MBs merged to form larger MBs with a diameter of ~40 μm. We also noted a color change of the *np*Fe^{III}-TA RPs suspension, which could be the result of oxidative degradation of TA, which led to the disassembly of the Fe^{III}-TA complexes (**Figure S7**).[23] Bubbles were not observed in the H_2O_2 solution without *np*Fe^{III}-TA RPs. To further prove the existence of O_2, *np*Fe^{III}-TA RPs (~0.043 mM Fe^{3+}) were mixed with different concentrations of H_2O_2 (pH 7.4, PBS buffer), and the generated O_2 was measured using an extracellular flux (XF) analyzer. Within the first 10 min, the generation of O_2 could not be measured due to the initialization process of the XF. Thereafter, the O_2 level increased dramatically for the next 20 min, reaching a maximum level of 315 mmHg (in 100 mM H_2O_2), and minimum level of 148 mmHg (in 0.5 mM H_2O_2). The generation of O_2 decreased 35 min after starting the experiment, and steady levels of O_2 were generated until the experiment ended at 70 min (**Figure 3b,c**). No increase of O_2 could be observed in *np*Fe^{III}-TA RPs without H_2O_2. The cumulative O_2 production was linearly correlated within a wide range of H_2O_2 concentrations (0–100 mM, R^2 = 0.96, and 0–5 mM, R^2 = 0.99).

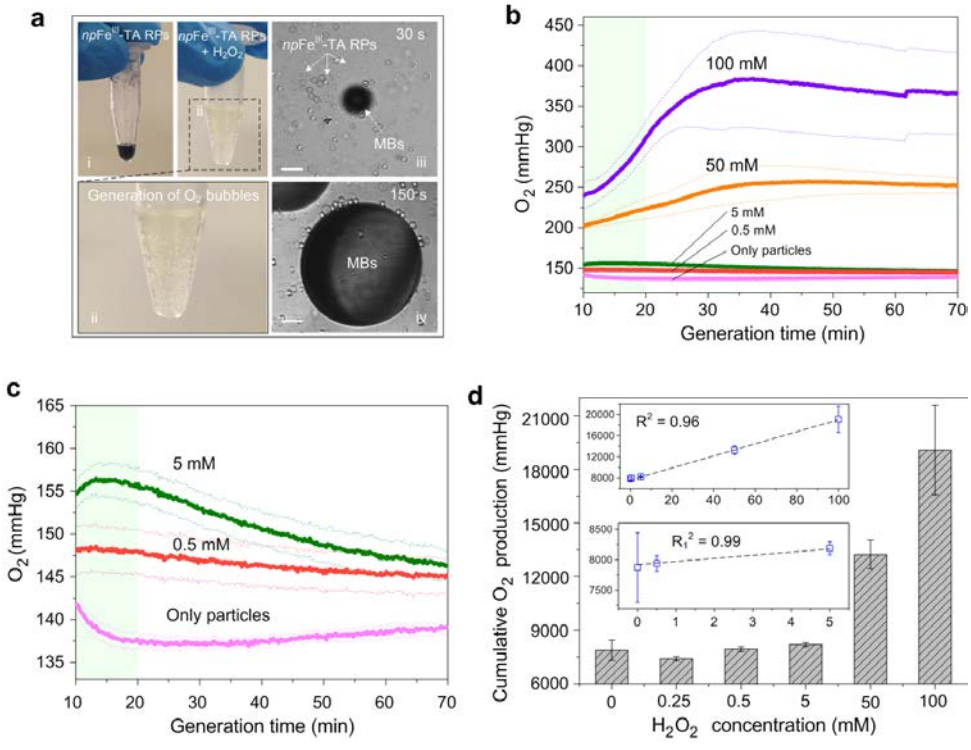

Figure 3. H_2O_2-dependent generation of O_2 MBs by *np*Fe^{III}-TA RPs *in vitro*. (a) *np*Fe^{III}-TA RPs suspension (i), mixture of *np*Fe^{III}-TA RPs and H_2O_2 in PBS buffer (ii), growth of MBs under DIC microscopy after mixing the *np*Fe^{III}-TA RPs and H_2O_2 for 30 s (iii) and 150 s (iv).

(b) and (c) Kinetics of O_2 production with different concentrations of H_2O_2: (b) full H_2O_2 concentration range (0 to 100 mM); and (c) low H_2O_2 concentration range (0 mM to 5 mM). The dashed lines represented the standard deviations. Data represent means ± SD, n = 3. (d) Linear increase of the cumulative O_2 production based on H_2O_2 concentration. Scale bars are 5.0 μm in the microscopy images.

GPx1$^{-/-}$ mice were chosen as a clinically relevant model to examine the potential of *np*Fe^{III}-TA RPs in the detection of endogenous H_2O_2 *ex vivo* and *in vivo* (**Figure 4**). WT mice were used as a negative control. GPx1 is an important antioxidant enzyme that forms part of the second-step of the antioxidant pathway in the conversion of H_2O_2 to H_2O.[24] GPx1$^{-/-}$ mice have a reduced capacity to remove H_2O_2, due to the complete knockout of GPx1 within both the mitochondria and the cytosolic compartments of the cell (**Figure 4a**).[25] Studies in WT mice have demonstrated high levels of GPx1 expression in organs such as the liver, and therefore GPx1$^{-/-}$ mice demonstrate elevated levels of H_2O_2 in various organs, particularly the liver. The elevated liver H_2O_2 levels make these mice an ideal model to investigate the *np*Fe^{III}-TA RPs for detecting H_2O_2. Initially, livers were isolated from the mice and placed on an imaging platform (**Figure 4b,c**). The *np*Fe^{III}-TA RPs (50 μL, ~0.86 mM Fe^{3+}) were then injected steadily into the *ex vivo* liver tissue by a micro-injector (**Figure S8**). An increased spot of US brightness was observed after injection, demonstrating the production of O_2 MBs resulting from the *np*Fe^{III}-TA RPs interacting with the elevated liver H_2O_2 levels for the GPx1$^{-/-}$ mice (**Figure 4d**). In contrast, no increased brightness was observed in the control WT mice, as determined by measuring the grayscale intensity in the region of interest for the acquired images (**Figure 4e,f**). For the GPx1$^{-/-}$ mice, the grayscale intensity increased after injection and reached a peak at 15 min, followed by a moderate decrease after 20 min. The decrease of grayscale intensity after the initial peak could be due to the diffusion of the MBs and the degradation of the *np*Fe^{III}-TA RPs after imaging. Lower concentrations of *np*Fe^{III}-TA RPs (50 μL, ~0.43 mM Fe^{3+}) were also injected into the liver, and the increased grayscale intensity correlated well with the injected dose (**Figure S9**).

With these promising *ex vivo* results, next we examined an *in vivo* model where we intravenously injected the *np*Fe^{III}-TA RPs (100 μL, ~0.86 mM Fe^{3+}) into WT and GPx1$^{-/-}$ mice (**Figure 4g**). To facilitate the injection, an incision was performed on the leg of the mice to allow the insertion of a catheter into the femoral vein. Similar to our previous study on MPNs,[14b] the *np*Fe^{III}-TA RPs accumulated in the liver and high brightness spots were visible 10 min after injection using US (**Figure 4h**). The intensity of these spots increased after

approximately 10 min, peaked at 25 min, and diminished at approximately 35 min post injection. No bright spots were observed in the WT control mice. Similar to our *ex vivo* experiments, we analyzed the acquired images and measured the grayscale intensity at the region of interest (**Figure 4i**). A significant increase in grayscale intensity was noted at 15, 20, and 25 min post injection in the GPx1$^{-/-}$ mice, while there was no increase in grayscale intensity for the control WT mice. The enhancement of US contrast agreed well with the *in vitro* XF experiments, which showed a dramatic increase of O_2 production in the initial 20 min, followed by a gradual decrease (**Figure 3b,c**).

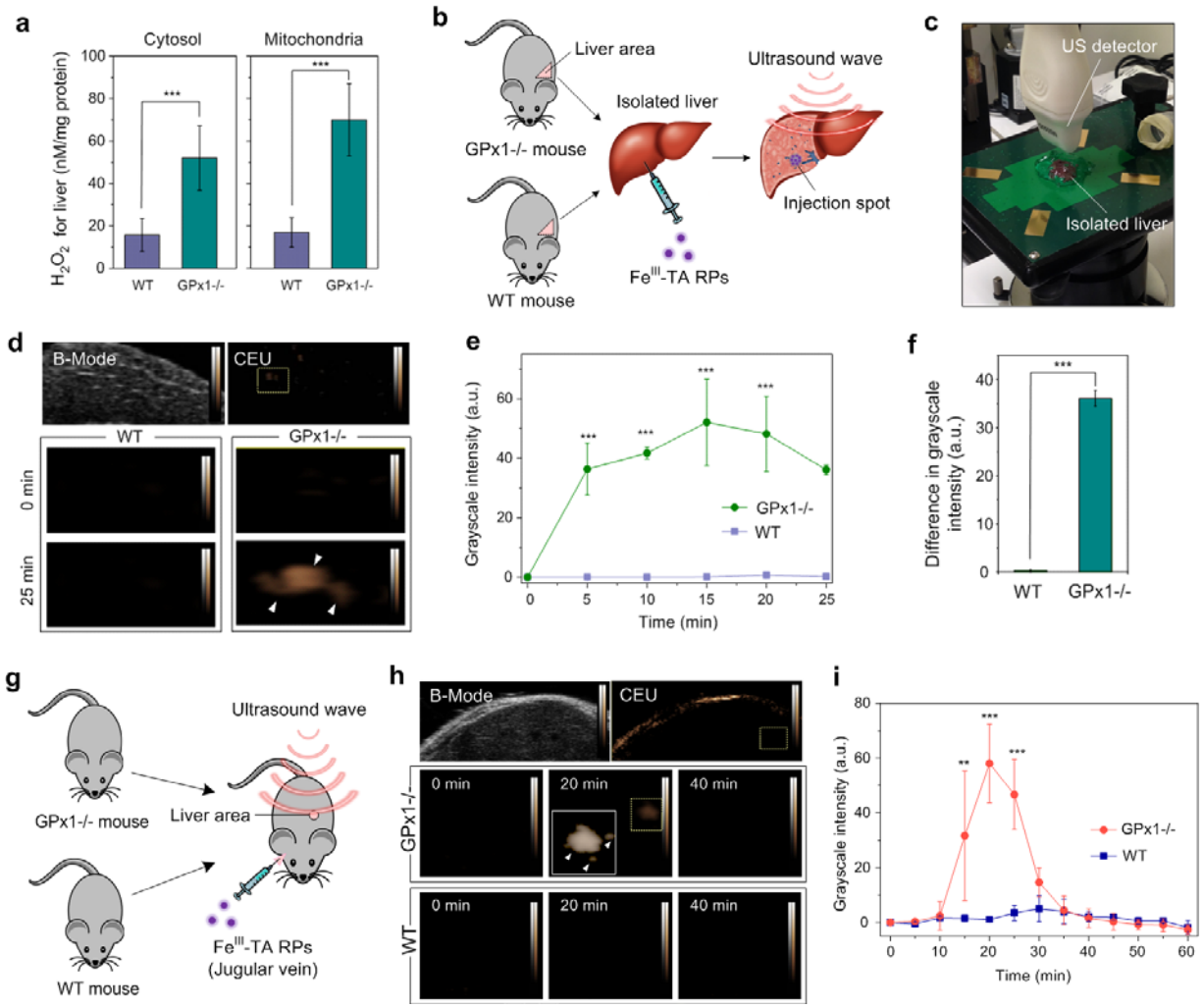

Figure 4. Enhanced ultrasound contrast resulting from the interaction of the *np*Fe^{III}-TA RPs with oxidative stress in mouse livers *ex vivo* and *in vivo* induced by GPx1 deficiency. (a) H_2O_2 concentrations in the GPx1$^{-/-}$ deficiency and WT mice, $^{***}P < 0.001$ (Student's t-test). (b) Schematic representation for the isolation of livers and the US probing of H_2O_2. (c) Photograph of the *ex vivo* US imaging setting. (d) Representative brightness mode (B-mode) and contrast

enhanced ultrasound (CEU) images of the mouse livers over time *ex vivo*. (e) Corresponding mean grayscale changes of the mouse livers *ex vivo* show the enhanced US contrast after 5 min injection. $^{***}P < 0.001$ (two-way ANOVA). (f) Quantitative image analysis of the CEU images of the mouse livers *ex vivo*. $^{***}P < 0.001$ (Student's t-test). (g) Schematic representation of the US probing of H_2O_2 *in vivo*. (h) Representative B-mode and CEU images of the mouse livers over time *in vivo*. The inset shows the area of interest with enhanced brightness and contrast. (i) Corresponding mean grayscale changes of the mouse livers *in vivo* shows enhanced US contrast 15 min after injecting the *np*Fe^{III}-TA RPs into the $GPx1^{-/-}$ mice. $^{**}P < 0.01$, $^{***}P < 0.001$ (two-way ANOVA). Data represents means ± SD, n = 3.

In summary, we have reported the facile and efficient formation of nanoporous metal-phenolic particles (*np*Fe^{III}-TA RPs) through the coordination complexation of a polyphenol (TA) and Fe^{3+}. The *np*Fe^{III}-TA RPs have highly nanoporous structures, formed by the nanostructural replication of nanoporous $CaCO_3$ template particles. The Fe^{3+} chelated in the phenolic ligands possess catalytic activity to breakdown H_2O_2 into O_2, accompanied by disassembly of the Fe^{III}-TA complexes at physiological pH. The cumulative production of O_2 is linearly related over a wide concentration range of H_2O_2 (0 to 100 mM), which ensures the nucleation of O_2 microbubbles (MBs). The *np*Fe^{III}-TA RPs were used to rapidly detect endogenous levels of H_2O_2 by US in $GPx1^{-/-}$ mice *ex vivo* and *in vivo*. Given the high biocompatibility of these materials (TA is an antioxidant and Fe^{3+} is an essential mineral), the *np*Fe^{III}-TA RPs provide various opportunities for advanced ultrasound imaging; from facilitating the preclinical investigation of physiological and pathological processes in biological systems to new theranostic methods in the process of clinical translation.

Supporting Information

Supporting Information is available from the Wiley Online Library. HOPE denotes an antioxidant trial of Heart Outcomes Prevention Evaluation, and GISSI denotes an antioxidant trial of Gruppo Italiano per lo Studio della Sopravvivenza nell'Infarto Miocardico (an Italian group for the study of the survival of Myocardial Infarction).

Acknowledgements

This research was conducted and funded by the Australian Research Council Centre of Excellence in Convergent Bio-Nano Science and Technology (project number CE140100036). This work was also

supported by the Australian Research Council under the Australian Laureate Fellowship (F.C., FL120100030) and Discovery Project (F.C., DP130101846) schemes, and by project grants (to C.E.H. and K.P.) and a Principal Research Fellowship (to K.P) from the National Health and Medical Research Council, as well as Fellowships from the National Heart Foundation (Career Development Fellowship to C.E.H. and Postdoctoral Fellowship to X.W.). This research was undertaken using equipment co-funded by the Ian Potter Foundation. The work was also supported in part by the Victorian Government's Operational Infrastructure Support Program. J.G. is grateful for a scholarship under the Chinese government award for outstanding self-financed students abroad by the China Scholarship Council. We acknowledge Dr. Derek Yuen (Oxidative Stress, Baker IDI Heart and Diabetes Institute, Australia), Dr. Ming Hu, Dr. Huanli Sun, Dr. Yunlu Dai, Katelyn Gause (Department of Chemical and Biomolecular Engineering, The University of Melbourne, Australia), and Fan Tian (School of Engineering, The University of Melbourne, Australia) for valuable discussions.

[1] N. Ardanaz, P. J. Pagano, *Exp. Biol. Med.* **2006**, *231*, 237.

[2] a) A. van der Vliet, Y. M. Janssen-Heininger, *J. Cell. Biochem.* **2014**, *115*, 427; b) M. P. Lisanti, U. E. Martinez-Outschoorn, Z. Lin, S. Pavlides, D. Whitaker-Menezes, R. G. Pestell, A. Howell, F. Sotgia, *Cell Cycle* **2011**, 10; c) N. V. Goncharov, P. V. Avdonin, A. D. Nadeev, I. L. Zharkikh, R. O. Jenkins, *Curr. Pharm. Des.* **2015**, *21*, 1134.

[3] R. Weinstain, E. N. Savariar, C. N. Felsen, R. Y. Tsien, *J. Am. Chem. Soc.* **2014**, *136*, 874.

[4] C.-K. Lim, Y.-D. Lee, J. Na, J. M. Oh, S. Her, K. Kim, K. Choi, S. Kim, I. C. Kwon, *Adv. Funct. Mater.* **2010**, *20*, 2644.

[5] W. Chen, Q.-Q. Ren, Q. Yang, W. Wen, Y.-D. Zhao, *Anal. Lett.* **2012**, 45, 156.

[6] F. Yang, S. Hu, Y. Zhang, X. Cai, Y. Huang, F. Wang, S. Wen, G. Teng, N. Gu, *Adv. Mater.* **2012**, *24*, 5205.

[7] N. Khaper, S. Bryan, S. Dhingra, R. Singal, A. Bajaj, C. M. Pathak, P. K. Singal, *Antioxid. Redox Signal.* **2010**, *13*, 1033.

[8] H. D. Sesso, J. E. Buring, W. G. Christen, T. Kurth, C. Belanger, J. MacFadyen, V. Bubes, J. E. Manson, R. J. Glynn, J. M. Gaziano, *J. Am. Med. Assoc.* **2008**, *300*, 2123.

[9] R. Fazel, H. M. Krumholz, Y. Wang, J. S. Ross, J. Chen, H. H. Ting, N. D. Shah, K. Nasir, A. J. Einstein, B. K. Nallamothu, *N. Engl. J. Med.* **2009**, *361*, 849.

[10] A. L. Klibanov, *Invest. Radiol.* **2006**, *41*, 354.

[11] F. Kiessling, S. Fokong, P. Koczera, W. Lederle, T. Lammers, *J. Nucl. Med.* **2012**, *53*, 345.

[12] B. A. Kaufmann, C. L. Carr, J. T. Belcik, A. Xie, Q. Yue, S. Chadderdon, E. S. Caplan, J. Khangura, S. Bullens, S. Bunting, *Arterioscler. Thromb. Vasc. Biol.* **2010**, *30*, 54.

[13] X. Wang, C. E. Hagemeyer, J. D. Hohmann, E. Leitner, P. C. Armstrong, F. Jia, M. Olschewski, A. Needles, K. Peter, I. Ahrens, *Circulation* **2012**, *125*, 3117.

[14] a) H. Ejima, J. J. Richardson, K. Liang, J. P. Best, M. P. van Koeverden, G. K. Such, J. Cui, F. Caruso, *Science* **2013**, *341*, 154; b) J. Guo, Y. Ping, H. Ejima, K. Alt, M. Meissner, J. J. Richardson, Y. Yan, K. Peter, D. von Elverfeldt, C. E. Hagemeyer, F. Caruso, *Angew. Chem. Int. Ed.* **2014**, *53*, 5546.

[15] F. Kiessling, S. Fokong, J. Bzyl, W. Lederle, M. Palmowski, T. Lammers, *Adv. Drug Deliv. Rev.* **2014**, *72*, 15.

[16] M. Oelze, S. Kroller-Schon, S. Steven, E. Lubos, C. Doppler, M. Hausding, S. Tobias, C. Brochhausen, H. Li, M. Torzewski, P. Wenzel, M. Bachschmid, K. J. Lackner, E. Schulz, T. Munzel, A. Daiber, *Hypertension* **2014**, *63*, 390.

[17] M. Torzewski, V. Ochsenhirt, A. L. Kleschyov, M. Oelze, A. Daiber, H. Li, H. Rossmann, S. Tsimikas, K. Reifenberg, F. Cheng, H. A. Lehr, S. Blankenberg, U. Forstermann, T. Munzel, K. J. Lackner, *Arterioscler. Thromb. Vasc. Biol.* **2007**, *27*, 850.

[18] P. Chew, D. Y. Yuen, N. Stefanovic, J. Pete, M. T. Coughlan, K. A. Jandeleit-Dahm, M. C. Thomas, F. Rosenfeldt, M. E. Cooper, J. B. de Haan, *Diabetes* **2010**, *59*, 3198.

[19] P. J. Crack, J. A. Taylor, J. B. de Haan, I. Kola, P. Hertzog, R. C. Iannello, *J. Cereb. Blood Flow Metab.* **2003**, *23*, 19.

[20] N. J. Flentjar, P. J. Crack, R. Boyd, M. Malin, J. B. de Haan, P. Hertzog, I. Kola, R. Iannello, *Exp. Neurol.* **2002**, *177*, 9.

[21] S. M. Tan, N. Stefanovic, G. Tan, J. L. Wilkinson-Berka, J. B. de Haan, *Invest. Ophthalmol. Vis. Sci.* **2013**, *54*, 555.

[22] Z. Zhao, L. Zhang, H. Dai, Y. Du, X. Meng, R. Zhang, Y. Liu, J. Deng, *Microporous Mesoporous Mater.* **2011**, *138*, 191.

[23] N. R. Perron, H. C. Wang, S. N. DeGuire, M. Jenkins, M. Lawson, J. L. Brumaghim, *Dalton Trans.* **2010**, *39*, 9982.

[24] J. B. de Haan, P. J. Crack, N. Flentjar, R. C. Iannello, P. J. Hertzog, I. Kola, *Redox Rep.* **2003**, *8*, 69.

[25] J. B. de Haan, C. Bladier, P. Griffiths, M. Kelner, R. D. O'Shea, N. S. Cheung, R. T. Bronson, M. J. Silvestro, S. Wild, S. S. Zheng, P. M. Beart, P. J. Hertzog, I. Kola, *J. Biol. Chem.* **1998**, *273*, 22528.

Nanoporous metal-phenolic particles are fabricated through the nanostructural replication of dense Fe^{III}-TA complexes in nanoporous $CaCO_3$ template particles. The *np*Fe^{III}-TA RPs have potential for the diagnostic detection of endogenous levels of H_2O_2 *ex vivo* and *in vivo* by ultrasound imaging, which is based on the catalytic activity of the coordinated Fe^{3+} in the particles to breakdown H_2O_2 to O_2 microbubbles.

Keywords: Hydrogen peroxide, metal-phenolic particles, and ultrasound imaging

Junling Guo, Xiaowei Wang, Darren C. Henstridge, Joseph J. Richardson, Jiwei Cui, Arpeeta Sharma, Mark A. Febbraio, Karlheinz Peter, Judy B. de Haan, Christoph E. Hagemeyer, and Frank Caruso

Nanoporous Metal-Phenolic Particles as Ultrasound Imaging Probes for Hydrogen Peroxide